Growth mechanism of silicene on Ag (111) determined by scanning tunneling microscopy measurements and ab initio calculations

R. Bernard, Y. Borensztein, H. Cruguel, M. Lazzeri, Geoffroy Prévot

Growth mechanism of silicene on Ag(111) determined by scanning tunneling microscopy measurements and *ab initio* calculations

R. Bernard,[1,2] Y. Borensztein,[1,2] H. Cruguel,[1,2] M. Lazzeri,[3] and G. Prévot[1,2,*]

[1]*Institut des NanoSciences de Paris, Université Paris 6, 4 place Jussieu, 75252 Paris CEDEX 05, France*

[2]*Institut des NanoSciences de Paris, UMR CNRS 7588, 4 place Jussieu, 75252 Paris CEDEX 05, France*

[3]*Institut de Minéralogie, de Physique des Matériaux, et de Cosmochimie, Sorbonne Universités, UPMC Université Paris 06, UMR CNRS 7590, MNHN, IRD UMR 206, 4 place Jussieu, Paris, France*

(Received 7 May 2015; revised manuscript received 16 June 2015; published 16 July 2015)

Scanning tunneling microscopy has been used to real-time study the growth of silicene on Ag(111) in the 200–533-K temperature range. We show that the growth mode depends strongly on the deposition temperature T. At $T = 300$ K and above, the formation of silicene results from the exchange between surface Ag atoms and Si atoms, which are inserted in the substrate top layer. Density functional theory calculations confirm that Si insertion is thermodynamically favored, and we propose an energetic model for explaining the observed growth processes as a function of T. For $T \geqslant 400$ K, ordered structures are observed as soon as silicene domains are large enough. With increasing coverage, disordered and dotted phases progressively transform into stable $(\sqrt{13} \times \sqrt{13})R13.9^\circ$ and (4×4) structures.

DOI: 10.1103/PhysRevB.92.045415 PACS number(s): 81.07.−b, 68.37.Ef, 71.15.Mb, 68.47.De

I. INTRODUCTION

The synthesis of bidimensional silicon films that would display electronic properties analog to those of graphene today attracts considerable interest, in particular for applications in microelectronics [1]. So-called silicene layers have been claimed to grow on various substrates, such as MoS_2, ZrB_2, ZrC_2, or Ir(111) [2], although, up to now, most of the studies have been performed on Ag(110) and Ag(111) substrates [3–18]. The interest for Ag substrates for silicene growth is related to: (i) the complete miscibility gap in the solid phase of the Ag-Si phase diagram, (ii) to a very good lattice matching since there is a ratio of 3/4 between the lattice constants of Si and Ag, and (iii) to a similar electronegativity of 1.9, leading to a small charge transfer between the layer and the substrate. Until recently, it was thus assumed that Si should grow on Ag substrates with negligible interactions. A structure identified as a "graphitic silicon layer" was first identified on Ag(100) [19]. Si stripes grown on Ag(110) where then described as silicene nanoribbons [3]. Finally, different structures observed on Ag(111) were described as silicene planes with various epitaxial relationships with the Ag(111) substrate, depending on substrate temperature and Si coverage. The best organized structure displays a (4×4) symmetry with respect to the Ag(111) [6–11,13–15,17]. Other ordered phases corresponding to $(\sqrt{13} \times \sqrt{13})R13.9^\circ$ [5–7,9,11,14,15,17,18], $(2\sqrt{3} \times 2\sqrt{3})R30^\circ$ [4,6,8,17], $(3.5 \times 3.5)R26^\circ$ [11], $(\sqrt{7} \times \sqrt{7})R19.1^\circ$ [6], and $(\sqrt{133} \times \sqrt{133})R4.3^\circ$ [20] reconstructions have been also identified. These structures have been described as Si atomic single layers organized in a honeycomb lattice on top of a (111) Ag plane with Si-Si interatomic distances close to the one predicted for free-standing silicene [8,10]. Additionally, a $(4/\sqrt{3} \times 4/\sqrt{3})$ phase has also been observed and attributed to the presence of two Si layers [5,11]. This superstructure also called $(\sqrt{3} \times \sqrt{3})$ with reference to the Si(111) (1×1) surface remains for thicker deposits [21,22].

However, recent experiments have shown that the Ag(110) surface reconstructs upon Si adsorption, even at room temperature [23], and facets at high Si coverage [24]. This was interpreted as a natural tendency for Ag(110) to reconstruct, Ag(110) being intermediate between Au(110) that spontaneously reconstructs and Cu(110) that does not [25].

On Ag(111), density functional theory (DFT) calculations have also shown that the interaction between Ag and Si leads to a strong modification of the electronic structure of silicene as compared to the one calculated for free-standing silicene [26]. In recent experiments, we have found that similar to the Ag(110) surface, the Ag(111) surface is not stable upon Si adsorption [27]. When silicene growth is performed for substrate temperatures around 460 K, Si incoming atoms exchange with Ag surface plane atoms, and these ejected Ag form new Ag terraces growing from the step edge. These findings indicate that, during deposition, the interaction between the Si and the Ag substrates is much more important than what was originally thought. Indeed, the formation of a Si-Ag surface alloy during growth is now also considered [20,28].

In the present paper, in order to understand the elementary steps involved in the growth of Si layers, we have used scanning tunneling microscopy (STM) for real-time follow-up Si/Ag(111) growth for substrate temperatures in the 200–533-K range, and we have compared the results to DFT calculations. We show that whereas a pseudo-layer-by-layer growth is observed at $T = 200$ K, Si atoms insert within the Ag(111) surface plane for $T \geqslant 300$ K. DFT calculations indicate that this atomic exchange is energetically favored. Released Ag atoms incorporate into step edges at low Si coverage or form additional islands at high Si coverage. From the evolution of the Si island density, we propose a growth mechanism for Si/Ag(111).

II. EXPERIMENTAL AND CALCULATIONAL DETAILS

Sample preparation and STM experiments have been performed in an ultra-high-vacuum system with a base pressure less than 1×10^{-10} mbar equipped with an Omicron

*Corresponding author: prevot@insp.jussieu.fr

variable temperature STM. The Ag(111) single crystal was prepared by several cycles of Ar ion sputtering ($P = 7 \times 10^{-5}$ mbar, 600 eV) and annealing ($T = 870$ K). Silicon was evaporated using an Omicron Nanotechnology e-beam evaporator installed in front of the STM with a flux $F \approx 0.1$ ML/h. Here, 1 monolayer (ML) corresponds to the coverage of a single (4×4) silicene layer, i.e., 1.125 times the atomic density of a Ag (111) plane, assuming the standard model of a silicene structure [10]. Note that this is also very close to the coverage of the $(\sqrt{13} \times \sqrt{13})R13.9^\circ$ and $(2\sqrt{3} \times 2\sqrt{3})R30^\circ$ structures [8]. STM imaging was performed in real time during Si evaporation. The pressure was always below 1×10^{-10} mbar during the experiments. Because of shadowing by the tip, we alternatively scanned two different regions of the sample, separated by approximately 1 μm. Thus, when one region was being scanned, the other one was fully exposed to the Si beam, which allowed us to follow the evolution of both regions during the growth process. Surface morphologies obtained in this way were identical to those observed on regions far from the shadow of the tip for similar coverage. Comparison between images of the same area performed at different times have been made by carefully correcting the STM images from the drift using a homemade procedure [29].

DFT calculations were performed with the two different approximations known as local density approximation (LDA) [30] and generalized gradient approximation (GGA) [31] by using the QUANTUM ESPRESSO package [32]. We used projector augmented-wave pseudopotentials from Ref. [33] and plane waves up to 30-Ry energy cutoff (240 Ry for the charge). A smearing approach [34] with broadening of 0.05 Ry was used. The Ag (111) surface was simulated with a supercell with four atomic layers and a vacuum thickness equivalent to six atomic layers. The in-plane periodicity was (4×4) and $(\sqrt{13} \times \sqrt{13})$ for the corresponding ordered structures, otherwise it was (2×2). Electronic integration was performed on a grid equivalent to the $12 \times 12 \times 1$ grid on the (1×1) cell. All these parameters were carefully tested for convergence (the reported energetics do not substantially change for larger supercells and thicker slabs). The in-plane lattice spacing was fixed at the theoretical equilibrium bulk lattice spacing (2.837 Å for LDA and 2.935 Å for GGA). The reported energetics corresponds to the structures obtained after full atomic relaxation (only the two bottom layers remained fixed at the bulk value).

III. RESULTS

A. Nucleation and growth

In this paragraph, we report STM observations of the nucleation and growth of the silicene layer as a function of the substrate temperature. In Fig. 1 is presented the evolution of the Ag surface with increasing Si deposition for $T = 200$ K. At low coverage, flat two-dimensional (2D) islands grow in the center of the terraces and at step edges. Their apparent height is 0.21 nm. They do not display any ordered structure (the reconstructions typically associated with Si are not observed). In addition to these islands that appear brighter on the image, some dark clusters are also visible, covering a much smaller fraction of the surface, as can be seen in the inset of Fig. 1(a). These minority dark clusters are likely due to inserted Si atoms,

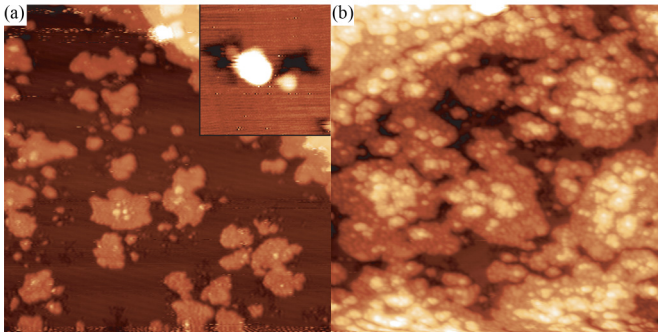

FIG. 1. (Color online) Growth of Si/Ag(111) at $T = 200$ K for increasing coverage. Size of the images (a) 86×86 nm^2 and (b) 43×43 nm^2. The size of the inset in (a) is 21×21 nm^2. Tunneling conditions: (a) -1.0 V and 30 pA and (b) 1.8 V and 30 pA.

which are predominantly observed at higher temperatures (see below). As the coverage increases, the islands coalesce. A second layer begins to grow before completion of the first layer as can be seen in Fig. 1(b) with a slightly larger apparent height (0.23 nm). This is much smaller than the interlayer spacing between biplanes of Si in the diamond structure (0.31 nm). However, the measured height could be different from the interlayer spacing, being affected by the different electronic structures of the successive layers.

For 300-K deposition, the evolution of the surface is completely different and is shown in Fig. 2. As soon as deposition begins, isolated dark spots are visible on the STM images [see the inset of Fig. 2(b)]. Successive images taken at 2-min intervals show that at this temperature, they are not very mobile: Almost all the spots are found at the same position. However, some of them have moved a few nanometers from their initial positions. Upon further Si exposure, the dark spots act as nucleation centers for the growth of 2D Si islands visible in Fig. 2(b). From the topographic images acquired at positive gap voltages (in the 0.5–1.8-V range), Si islands appear below the Ag(111) terrace on which they form. Depending on the tip termination, they are either found 0.06 or 0.13 nm below the Ag terrace plane. Such islands nucleate mainly within the terraces and less at step edges. In parallel, the step edges also show a

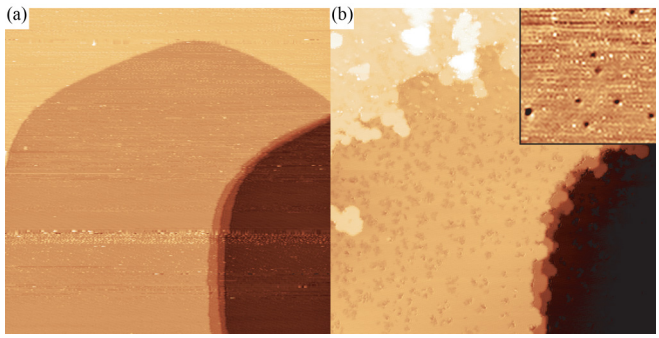

FIG. 2. (Color online) Growth of Si/Ag(111) at 300 K. (a) Bare surface, the size of the image is 150×150 nm^2. (b) The same region after deposition of a small coverage of Si. The inset shows a (21×21)-nm^2 area at the beginning of Si evaporation. Tunneling conditions: 1.8 V and 20 pA.

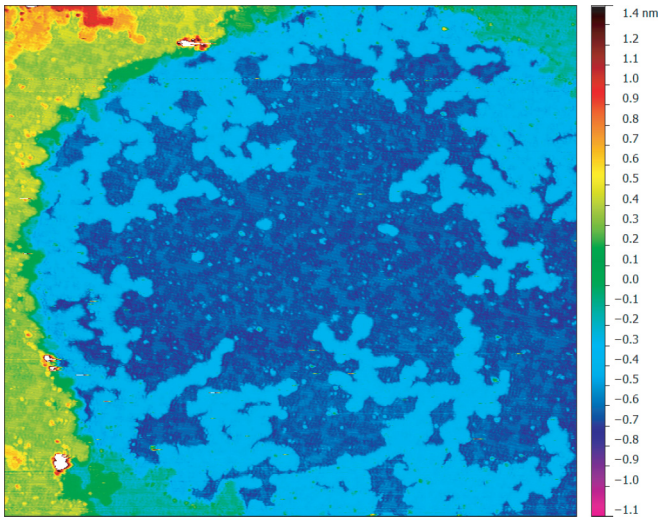

FIG. 3. (Color online) Growth of Si/Ag(111) at 300 K. The vertical color scale goes from blue (lower terrace) to red (upper terrace). The size of the image is $200 \times 180\,\mathrm{nm}^2$. Tunneling conditions: 1.8 V and 20 pA.

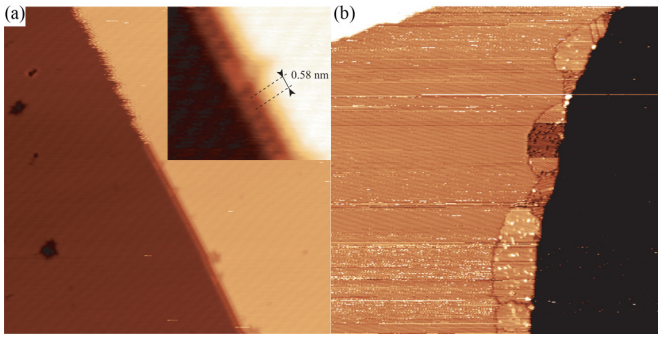

FIG. 4. (Color online) (a) Faceting and $\times 2$ reconstruction of a Ag step at the beginning of Si growth on Ag(111) at $T = 400\,\mathrm{K}$. The inset shows a detailed view of the step reconstruction. The size of the image is $43 \times 43\,\mathrm{nm}^2$. (b) The growth of the Si domain at a step edge at 533 K. The size of the image: $160 \times 160\,\mathrm{nm}^2$. Tunneling conditions: (a) 1.5 V and 30 pA and (b) 1.5 V and 50 pA.

significant modification. The comparison between Figs. 2(a) and 2(b) shows that simultaneous to the growth of Si islands, fingers appear at step edges. They are at the same height as the upper terrace and display the same atomic structure, indicating that they are constituted by Ag. The comparison between consecutive images performed at the same position demonstrates that these fingers issue from the growth of the upper terrace at the expense of the lower terrace. This phenomenon was already observed during Si deposition on Ag(110) at room temperature [23] and on Ag(111) at 440−480 K [35]. Such features result from the exchange between Si atoms and Ag atoms of the surface plane. Ejected Ag atoms diffuse towards the steps and contribute to the advance of the step edges. Thus, the dark spots observed at the beginning of the growth are Si atoms inserted within the Ag surface plane, which act as nucleation centers for the growth of inserted Si islands. As the coverage increases, both Ag fingers and Si inserted islands grow with a dendritic shape, and additional Ag islands form within the terraces (see Fig. 3). As can be seen in Fig. 3, these growing Ag structures fill the gaps between the Si islands on the terraces.

For deposition at substrate temperatures equal or higher than 400 K, the evolution of the surface in the very first stages of Si evaporation is quite different (Fig. 4). As soon as evaporation begins, Ag step edges facet towards ⟨110⟩ directions as already reported [27]. Along these step edges, the periodicity is equal to twice the Ag-Ag distance (0.58 nm) as can be seen in the inset of Fig. 4(a). We have never observed this faceting at 300 K. These observations are in agreement with STM studies after Si deposition on Ag(110) which showed faceting of the (110) surface into a (211) surface composed by small (111) terraces with the same $\times 2$ periodicity along the $[1\bar{1}0]$ step edges separating the terraces [24]. Figure 4(a) shows the evolution of such a step edge at the beginning of Si evaporation. In the upper part of the image, the step is free to move and appears frizzy due to the motion of the edge in the time interval between the acquisitions of two consecutive lines. In the lower part of the image, the presence of Si atoms has induced the step $\times 2$ reconstructionwith a few defects, and the step edge motion is completely blocked.

The observation of large-scale images shows that straight portions of step edges with $\times 2$ reconstruction may extend over 100 nm. The fact that the large fluctuations in the step edge position (observed prior evaporation) are blocked by Si indicates that each straight portion of a step is related to the $\times 2$ reconstruction developing from a single nucleus. This implies that Si atoms can easily diffuse along the step edges, thereby contributing to the propagation of the $\times 2$ reconstruction.

The faceting and reconstruction of step edges are also observed on the Ag fingers and Ag islands which grow during Si deposition. They display faceted shapes, which are less and less dendritic as temperature increases and grow until their sides are entirely covered by Si, forming the $\times 2$ reconstruction. Thus, they form and grow during a limited time. From the observation of large-scale images ($500 \times 500\,\mathrm{nm}^2$, not shown here), we conclude that the growth duration of a given Ag domain (finger or island) decreases with temperature: At high temperatures, large Ag domains form during a short interval of time whereas the density of growing Ag domains decreases. This indicates that Ag atoms diffuse over long distances to grow these domains, and this is compatible with the very small activation barrier for Ag diffusion on Ag(111) [36].

At 400 K, the dark spots which correspond to inserted Si atoms are found to be mobile. We have taken successive images of (50×50)-nm^2 areas that show that almost all spots have moved during the time interval of 2 min. At 440 K and above, such spots are rarely observed.

As already observed at 300 K, Si-inserted islands form within the terraces. At 400 K and above, Si domains also grow from step edges in the upper terrace and form strips [see Fig. 4(b)]. We always observed that there exists, on the upper terrace, a region near the step where no isolated Si island nucleates [see also Fig. 5(b)]. This can be interpreted by the fact that since Si domains act as sinks for Si atoms, there exist, near these domains, a region for which the density of Si atoms is lower and for which the probability of nucleation is reduced. Conversely, in the lower terraces, islands are observed

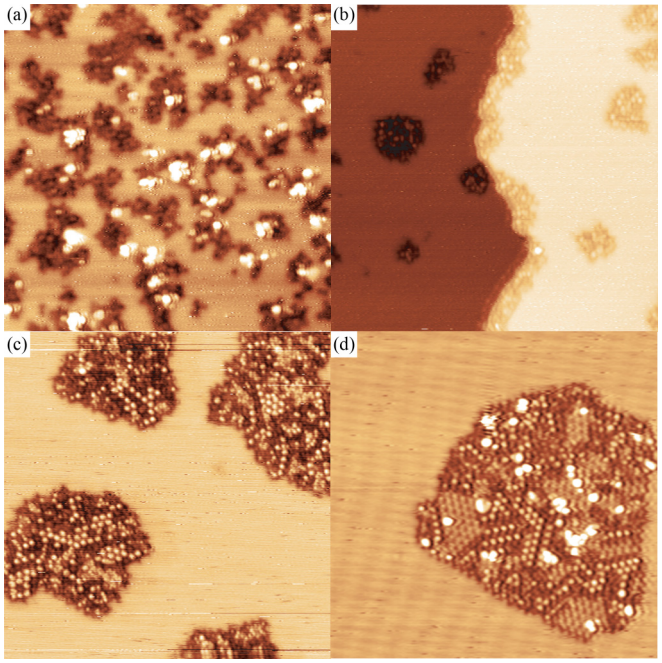

FIG. 5. (Color online) Morphology of small Si domains at different temperatures: (a) 300 K, (b) 400 K, (c) 440 K, and (d) 480 K. The size of the images is $43 \times 43\,\text{nm}^2$. Tunneling conditions: (a) 1 V and 20 pA, (b) and (c) 1.5 V and 30 pA, and (d) 1.5 V and 70 pA.

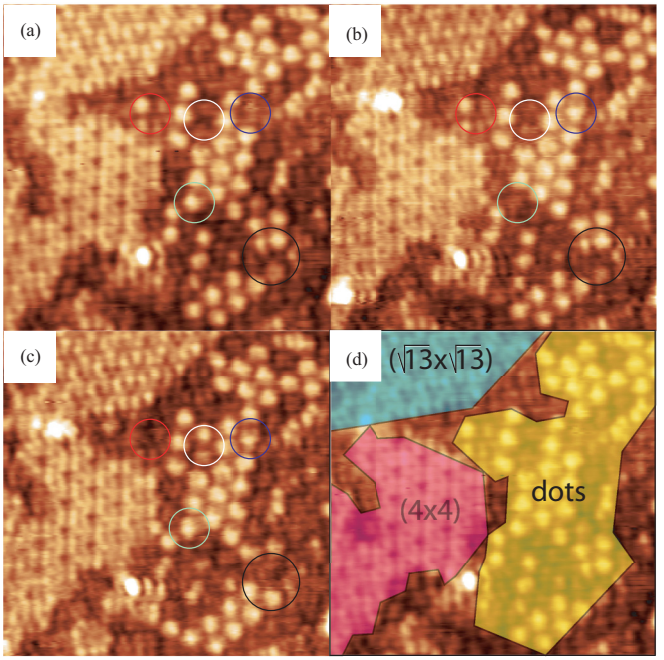

FIG. 6. (Color online) (a)–(c) Evolution of Si domains at $T = 480\,\text{K}$ during Si growth. The (4×4) and $(\sqrt{13} \times \sqrt{13})R13.9^\circ$ domains are stable. The positions of the dots that move from one image to another are indicated by circles. The size of the images is $13 \times 13\,\text{nm}^2$. The positions of the ordered domains are indicated in (d). Tunneling conditions: 1.5 V and 150 pA.

to nucleate near the step. This indicates that the Si strips at step edges are formed by Si atoms coming from the upper terrace.

As the temperature increases, the proportion of Si domains that have grown from a step (i.e., strips) increases and reaches 100% at 533 K. Even on terraces that are 200-nm wide, no Si islands nucleate within the terraces [see Fig. 4(b)].

B. Structure of the Si domains

Figure 5 presents high-resolution STM images of Si domains for different substrate temperatures. The comparison shows that the islands become larger and more ordered at higher temperatures and adopt a more triangular shape with boundaries along ⟨111⟩ directions.

At 300 K, no ordered structure can be found in the Si islands, but protrusions around 1 nm apart are clearly visible within the islands. For a growth temperature equal or higher than 400 K, ordered structures form in the Si islands and strips. Three kinds of structures are clearly identified (see Fig. 6 for a detailed view). From the angle and distance measurements, regions with (4×4) and $(\sqrt{13} \times \sqrt{13})R13.9^\circ$ structures are deduced. A structure formed by apparent dots also appears with a period around $1.00 \pm 0.02\,\text{nm}$, in agreement with possible $(\sqrt{13} \times \sqrt{13})R13.9^\circ$ of a different type [6,8,18,37] or $(3.5 \times 3.5)R26^\circ$ [11] reconstructions previously proposed. However, no specific orientation with respect to the substrate is clearly found for this latter structure. In addition to these ordered structures, some parts of the Si islands do not display long-range ordering.

The temperature dependence of the ordered structures observed has already been related. For a substrate temperature below 533 K and coverage less than one monolayer, (4×4) and $(\sqrt{13} \times \sqrt{13})R13.9^\circ$ structures are usually observed [8,11,17]. The question of whether a single structure can cover the whole substrate is still open. It has been assumed that a pure (4×4) layer could be obtained if the sample temperature was 423 K [8] or 493 K [10]. We have never obtained a single phase of silicene on Ag(111). The proportion of the different regions as a function of temperature is given in Table I for the completion of the monolayer.

The relative proportion between the different regions depends not only on the sample temperature, but also on the coverage. For 533 K, nearly only $(\sqrt{13} \times \sqrt{13})R13.9^\circ$ and (4×4) structures form during deposition. The Si strips are well ordered up to their boundaries. For $T = 480\,\text{K}$, the Si islands begin to order as soon as their size is larger than a few tens of nanometers [Fig. 5(d)]. Dotted phase and disordered regions are also present for submonolayer coverage. They are progressively replaced by $(\sqrt{13} \times \sqrt{13})R13.9^\circ$ and (4×4) structures. At the completion of the monolayer, ordered structures cover practically all the surface. At $T \leqslant 440\,\text{K}$,

TABLE I. Proportion of the structures observed at the completion of the monolayer for growth at different substrate temperatures.

Temperature (K)	(4×4) (%)	$(\sqrt{3} \times \sqrt{3})R13.9^\circ$ (%)	Dotted (%)	Disordered (%)
533	40	60	< 1	< 1
480	32	64	1	3
440	28	41	21	10

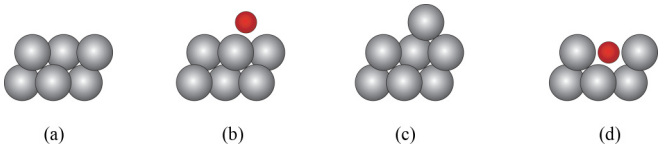

FIG. 7. (Color online) Atomic configurations tested by DFT. (a) Clean Ag(111) surface, (b) one Si atom adsorbed on the top of the surface, (c) one Ag atom on the top of the surface, and (d) one Si atom inserted in the surface.

dotted and disordered regions remain up to the completion of the monolayer.

The observation of $(\sqrt{13} \times \sqrt{13})R13.9^\circ$ and (4×4) regions shows that, once formed, these structures are stable during evaporation. They do not evolve towards disordered or differently ordered structures. However, it may happen that they are replaced with additional Ag terraces formed during the Si growth, but such modifications are scarce [27]. On the contrary, the dotted phase evolves continuously during evaporation. For example, dots can be replaced with $(\sqrt{13} \times \sqrt{13})R13.9^\circ$ and (4×4) structures [27]. Between consecutive STM images, some dots have appeared, whereas other have disappeared. Such modifications are visible in Fig. 6 where the moving dots are indicated by circles. The appearance and disappearance of these dots are related to the mobility of one or several atoms, and thus they question the nature of this dotted phase.

C. Simulation results

The various reconstructions found for silicene layers on Ag(111) have been intensively studied by DFT [5,7,9–12,18,26], and we have first checked that for the monolayer coverage, we could recover the stability of the (4×4) and $(\sqrt{13} \times \sqrt{13})$ structures. We have then focused our calculations on the energetics of Si atoms in the initial stage of deposition. The different configurations computed are shown in Fig. 7.

We have first calculated the energy of the clean surface E_{cl}^N (N is the number of atoms in the slab) [Fig. 7(a)] and the energy E_{blk}^1 of one Ag atom in the bulk, i.e., the Ag cohesive energy. We have then considered: (i) one Si atom adsorbed on the top of the surface [Fig. 7(b)], (ii) one Ag atom on the top of the surface [Fig. 7(c)], and (iii) one Si atom inserted in the surface [the Si atom substitutes one Ag atom of the first surface layer, Fig. 7(d)]. The energies of the three systems are called E_{Si}^{N+1}, E_{Ag}^{N+1}, and E_{Si}^{N}, respectively (in the third case there are $N-1$ Ag atoms and one Si atom). In both cases (i) and (ii), the most stable configuration is obtained by setting the adatom on the hollow fcc site.

By using DFT, we have calculated the energy difference between the atomic configuration before and after insertion of a Si atom on the surface by exchanging with a Ag atom: $\Delta E = (E_{\mathrm{Si}}^{N+1} - E_{\mathrm{Si}}^{N}) - (E_{\mathrm{Ag}}^{N+1} - E_{cl}^{N})$. From GGA calculations, which are expected to provide the most reliable results, we have $E_{ad} = 0.67$ and $\Delta E = +0.11$ eV. The positive sign of ΔE means that the insertion of a Si atom on the surface is favored with respect to a Si atom lying on the top of the surface. On the other hand, according to LDA calculations, $E_{ad} = 0.97$ and $\Delta E = -0.08$ eV. The difference between the GGA and the LDA results gives an idea of the precision of DFT for this kind of energy difference.

The insertion of a Si atom on the surface is also favored by the fact that the resulting Ag adatom thus created can diffuse towards a kink on a step edge, leading to a reduction in the system energy by E_{ad}. The creation energy of one Ag adatom on the surface is defined as $E_{ad} = E_{\mathrm{Ag}}^{N+1} - E_{cl}^{N} - E_{blk}^{1}$. One thus obtains an energy difference between a configuration with a Si adatom on the surface and a Si atom inserted on the surface of $E_{ad} + \Delta E = 0.78$ eV (GGA) or 0.89 eV (LDA). This large energy difference is in good agreement with the experimental observations.

IV. DISCUSSION

A. Alloy formation

Both STM experiments and DFT results show that the formation of a Si-Ag surface alloy is thermodynamically favored for low Si coverage. Such alloy formation has been observed for monolayer coverage on surfaces of metals that form bulk silicides. For example, room-temperature deposition of Si on Cu(110) leads to the formation of a $c(2 \times 2)$ surface alloy [38]. A $(\sqrt{19} \times \sqrt{19})R23.4^\circ$ surface alloy has also been observed after Si deposition on Pt(111) at 750 K [39]. In this case, DFT calculations also show that the protrusions visible in STM images correspond to Pt atoms, not to Si ones.

Surface alloy formation has also been observed during Si deposition on metals for which no ordered bulk silicide exists. This is the case for example for Si/Au(110) for which a $c(2 \times 2)$ phase, corresponding to an ordered surface alloy, forms during deposition at 673 K [40]. However, in this case, the substrate temperature during deposition is above the eutectic temperature so that alloying is not surprising. The Si/Ag(111) system can also be compared to Ge/Ag(111). Despite a low solubility of Ge in Ag at 300 K, Ge deposition on a Ag(111) surface at room temperature has been shown to induce the formation of a Ag_2Ge surface alloy with a $(\sqrt{3} \times \sqrt{3})R30^\circ$ structure [41]. This is very similar to what is observed for Si deposition, except that, for Si/Ag(111), ordered structures are only found if the substrate temperature is above 440 K.

As already reported, various ordered Si/Ag(111) superstructures have been identified. These structures have been described as Si atomic single layers organized in a honeycomb lattice on top of a (111) Ag plane with Si-Si interatomic distances close to the one predicted for free-standing silicene [8,10]. Structural analyses performed on the (4×4) structure by reflection high-energy positron diffraction [42] and low-energy electron diffraction [16] confirm the proposed model. On the contrary, a surface alloy model has been recently proposed for the $(\sqrt{133} \times \sqrt{133})R4.3^\circ$ [20] reconstruction that forms at 620 K, based on DFT calculations and Auger measurements. Thus, some of the observed ordered phases could correspond to surface alloys. In particular, this might be the case for the dotted phase which appears to be not stable upon further Si evaporation.

B. Nucleation and growth

In the following, we discuss our STM results in relation with the theory of nucleation and growth. Quantitative information can be obtained from the evolution of island density

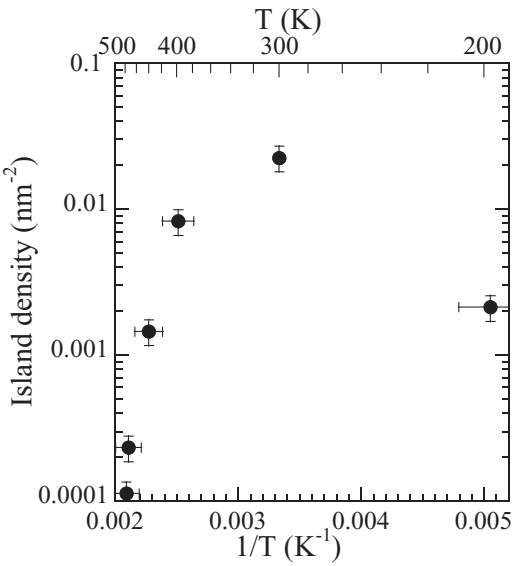

FIG. 8. Evolution of the island density as a function of the inverse of the temperature.

with temperature. In the classical theory of nucleation and growth [43], atoms adsorb on a surface, diffuse, and nucleate with other atoms to form stable clusters. Up to a critical size, clusters are unstable, i.e., they have a larger probability to decrease than to increase. Above the critical size, they have a larger probability to increase. Using analytical mean-field equations for describing diffusion, nucleation, and growth, the evolution of the island density can be determined. After a short initial rise (nucleation regime), the island density becomes nearly constant (growth regime) up to the coalescence regime. The island density in the growth regime is proportional to $(F/D)^{n/(n+2)}$, where D is the diffusion coefficient and where F is the atomic flux [43]. n is the number of atoms in the critical nucleus, i.e., the largest unstable cluster. Assuming that diffusion is thermally activated with the activation energy E_j, the diffusion coefficient can be written in the form $D = a^2\nu_0 \exp(-E_j/kT)$ where a is an interatomic distance and where ν_0 is an attempt frequency. Thus, the evolution of the island density on an Arrhenius plot should be linear as a function of $1/T$ with a positive slope related to the activation energy of the diffusion coefficient: The higher the temperature, the lower the island density.

Figure 8 shows the evolution of the Si island density on the terraces in the initial stage of growth as measured from the STM images as a function of the growth temperature in the 200−480-K temperature range. For $T = 533$ K, no islands are observed, Si domains nucleating only at step edges. The density does not increase exponentially with the inverse of temperature in the complete temperature range studied but only for temperatures higher than 300 K. The observed behavior with a "Λ shape" is thus far from the prediction of the classical theory. In particular, for low temperatures, the curve increases with increasing temperature, reaching a relative maximum for 300-K deposition. This unexpected behavior must be related to the fact that for low-temperature deposition ($T = 200$ K), Si atoms likely remain above the Ag surface plane, contrary to what is observed at 300 K and above where Si atoms insert within the surface plane.

Such a transition between different temperature regimes has already been observed for homoepitaxy and heteroepitaxy on metal surfaces [44–47]. Also in these systems, deposited atoms may remain above the surface or may insert, depending on the deposition temperature. For example, the Co/Cu(100) system displays a "N shape" of the Arrhenius plot of the island density [35]. We suggest that the Λ shape observed here for Si/Ag(111) corresponds to the high- and middle-temperature regimes observed for Co/Cu(100). In another system, Ni/Ag(111), a "V shape" of the Arrhenius plot is obtained, which corresponds to the middle- and low-temperature regimes in Co/Cu(100) [46]. This latter behavior is explained by the competition between two alternative nucleation mechanisms in which the nucleation center is associated with: (i) two diffusing atoms meeting on the top of the surface and (ii) one atom inserted within the surface. The inserted atom is assumed to be immobile. At low temperatures, the first mechanism is dominant, and the island density decreases with increasing temperature as expected from the classical nucleation theory. In the high-temperature regime, insertion occurs easily, and the second mechanism is dominant. Since inserted atoms are immobile, the island density increases with increasing temperature.

In the present case at $T = 200$ K, Si atoms diffuse on the surface by performing jumps which are thermally activated. At this low temperature, we can assume that Si dimers which form when two Si atoms meet are stable and act as nucleation centers for further growth ($n = 1$). Using $D = a^2\nu_0 \exp(-E_j/kT)$ where a is the Ag-Ag interatomic distance and where ν_0 is on the order of 10^{13} Hz [48], from the Si island density we obtain $E_j \approx 0.26$ eV [activation energy for Si diffusion by jumps on Ag(111)]. On the contrary, at 300 K, inserted isolated atoms are observed at the very initial stage of the deposition, whereas no Si clusters are visible above the surface, meaning that all Si atoms are inserted in the Ag surface in the submonolayer regime. This indicates that insertion occurs before nucleation of stable dimers, leading to a higher island density. At higher temperatures, the mechanism is similar with mobility of the inserted Si atoms, leading to a classical Arrhenius law with a positive slope.

From the transition temperature between these two regimes, we estimate the activation barrier for insertion. Since insertion (Si exchange with Ag atoms) does not occur at low temperatures, the energy barrier for insertion E_{in} must be higher than E_j. A schematic of the different involved processes is presented in Fig. 9. Thus, an isolated Si atom can perform several jumps before exchanging with a Ag atom. Assuming

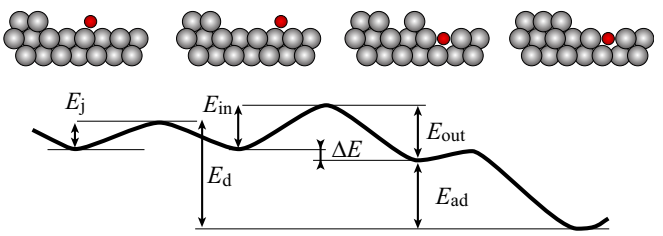

FIG. 9. (Color online) Schematic of the energy landscape for a Si atom adsorbed on the Ag(111) surface.

that the jump and the insertion process have the same attempt frequency, the mean number of jumps $\bar{N}_j$ performed before insertion is [49] as follows:

$$\bar{N}_j = \exp\left(\frac{E_{\text{in}} - E_j}{kT}\right), \quad (1)$$

and the distance traveled on the surface is proportional to $\sqrt{\bar{N}_j}$.

At $T = 200$ K, Si atoms nucleate above the surface before inserting. This indicates that the number of jumps needed to reach a nucleation center is less than the mean number of jumps performed before insertion. From the measured island density, we obtain that the mean distance between islands that have nucleated is equal to 23 nm, i.e., 80 interatomic distances. We thus obtain that $\exp(\frac{E_{\text{in}}-E_j}{2kT}) > 80$, which corresponds to $E_{\text{in}} - E_j > 0.15$ eV, hence $E_{\text{in}} > 0.41$ eV.

At $T = 300$ K, inserted Si atoms are observed before clusters can form on top of the surface. Moreover, from the STM observations, inserted Si atoms do not move. Thus, the islands grow due to the incorporation of diffusing Si adatoms which are eventually trapped at their edges and inserted on the surface. This indicates that for Si adatoms, the barrier for detachment from a Si island is higher than the barrier for insertion in this island. This is corroborated by the fact that the few dark clusters visible at $T = 200$ K and interpreted as inserted Si islands contain several Si atoms [inset of Fig. 1(a)]. It has already been proposed for Fe/Cu(100) that the barrier for insertion of an adatom in an inserted island could be lower than E_{in}, the one found for an isolated atom [44].

In the stationary regime, the number of jumps performed before insertion is roughly the number of jumps needed to reach a nucleation center. From the measured island density, we obtain that the mean distance between islands that have nucleated is 7 nm, i.e., 25 interatomic distances. We thus obtain $\exp(\frac{E_{\text{in}}-E_j}{2kT}) = 25$, which corresponds to $E_{\text{in}} - E_j = 0.17$ eV, hence $E_{\text{in}} = 0.43$ eV. This is coherent with the previous evaluation.

For growth at a substrate temperature equal or higher than 400 K, our STM observations show that the inserted Si atoms are mobile. Thus, we observe a decrease in island density with increasing temperature. This corresponds to the classical regime of the nucleation and growth theory (and is contrary to what is expected when inserted atoms are immobile). The evolution of island density for temperatures equal to or higher than 400 K can be fitted by an Arrhenius curve with apparent activation energy $E_{\text{app}} = 0.84 \pm 0.05$ eV. In the classical nucleation theory, it corresponds to $E_{\text{app}} = \frac{n}{n+2}E_d$, where E_d is the activation energy for diffusion of the inserted Si atoms. Thus, $0.84 \text{ eV} \leqslant E_d \leqslant 2.52$ eV, depending on the value of n, from infinite to 1.

Whatever the value of n, the value of E_d is quite large and could correspond to the barrier needed for removal of Si atoms from the Ag surface plane. In that case, Si-inserted atoms would diffuse by a three-step process: exchange with Ag adatoms, jumps on the surface, and reinsertion. For $\bar{N}_j \gg 1$, the diffusion coefficient associated with this process can be written as [35,49] $D = a^2 \bar{N}_j \nu_0 \exp(-\frac{E_{ad}}{kT}) \exp(-\frac{E_{\text{out}}}{kT})$, where E_{out} is the activation energy for an exchange between an inserted Si atom and a Ag adatom and E_{ad} is the creation energy of a Ag adatom on the surface. Using Eq. (1), one thus obtains

$$D = a^2 \nu_0 \exp\left(-\frac{E_{ad}}{kT}\right) \exp\left(-\frac{E_{\text{out}}}{kT}\right) \exp\left(\frac{E_{\text{in}} - E_j}{kT}\right). \quad (2)$$

From DFT calculations, we have obtained $E_{ad} = 0.67$ eV. Moreover, E_{in} and E_{out} are related through: $E_{\text{out}} = E_{\text{in}} + \Delta E$ where the energy difference between the atomic configuration before and after insertion is $\Delta E = 0.11$ eV. This leads to $D \approx a^2 \nu_0 \exp(-\frac{E_d}{kT})$ with $E_d = E_{ad} + \Delta E + E_j = 1.04$ eV. This value is thus in the range experimentally determined and, from the expression of the apparent activation energy, indicates that n is large, on the order of a few units. This value is also very coherent with the measured mobility of inserted Si atoms. At $T = 300$ K, $\nu_0 \exp(-\frac{E_d}{kT}) \approx 3.10^{-5}\ \text{s}^{-1}$. During the time interval between two consecutive images ($\approx$120 s), inserted Si atoms, most likely, do not move. At $T = 400$ K, $\nu_0 \exp(-\frac{E_d}{kT}) \approx 0.8\ \text{s}^{-1}$, and during the same time interval, all inserted Si atoms have moved through the three-step process mentioned above. There is thus a remarkable agreement between our energetic model and the experimental observations.

V. CONCLUSION

In conclusion, we have performed an extensive STM investigation of the growth of silicene upon the Ag(111) surface at different temperatures. Our real-time observations demonstrate that during deposition the interaction between the Si atoms and the Ag substrate is much more important than was previously thought. At 300 K and above, the Si atoms are exchanged with Ag atoms and are inserted within the top Ag layer, whereas at lower temperatures they remain above the Ag surface. The released Ag atoms diffuse on the surface and eventually attach to the step edges or form new Ag islands. Such exchange behavior is confirmed by DFT calculations which show that Si insertion is energetically favored. We have furthermore developed an energetic model which allowed us to explain the experimentally observed nucleation and growth processes at the different temperatures. This model shows the competition between two modes of growth, resulting in a specific variation in the island density with temperature.

Finally, at high temperatures, Si islands are progressively developing with some parts displaying the $(\sqrt{13} \times \sqrt{13})R13.9°$ and (4×4) structures, which are stable during evaporation, and other parts displaying a disordered phase and a dotted phase, which are not stable and progressively transform into the two more stable phases. In particular, some of the observed dots appear to be slightly mobile on the surface. Our results therefore question the exact structure of the different phases of silicene on Ag(111) for which possible alloying with Ag should be considered.

[1] L. Tao, E. Cinquanta, D. Chiappe, C. Grazianetti, M. Fanciulli, M. Dubey, A. Molle, and D. Akinwande, Nat. Nanotechnol. **10**, 227 (2015).

[2] L. Meng, Y. Wang, L. Zhang, S. Du, R. Wu, L. Li, Y. Zhang, G. Li, H. Zhou, W. A. Hofer, and H.-J. Gao, Nano Lett. **13**, 685 (2013).

[3] B. Aufray, A. Kara, S. Vizzini, H. Oughaddou, C. Léandri, B. Ealet, and G. Le Lay, Appl. Phys. Lett. **96**, 183102 (2010).

[4] B. Lalmi, H. Oughaddou, H. Enriquez, A. Kara, S. Vizzini, B. Ealet, and B. Aufray, Appl. Phys. Lett. **97**, 223109 (2010).

[5] L. Chen, C.-C. Liu, B. Feng, X. He, P. Cheng, Z. Ding, S. Meng, Y. Yao, and K. Wu, Phys. Rev. Lett. **109**, 056804 (2012).

[6] D. Chiappe, C. Grazianetti, G. Tallarida, M. Fanciulli, and A. Molle, Adv. Mater. **24**, 5088 (2012).

[7] B. Feng, Z. Ding, S. Meng, Y. Yao, X. He, P. Cheng, L. Chen, and K. Wu, Nano Lett. **12**, 3507 (2012).

[8] H. Jamgotchian, Y. Colignon, N. Hamzaoui, B. Ealet, J. Y. Hoarau, B. Aufray, and J. P. Bibérian, J. Phys.: Condens. Matter **24**, 172001 (2012).

[9] C.-L. Lin, R. Arafune, K. Kawahara, N. Tsukahara, E. Minamitani, Y. Kim, N. Takagi, and M. Kawai, Appl. Phys. Express **5**, 045802 (2012).

[10] P. Vogt, P. De Padova, C. Quaresima, J. Avila, E. Frantzeskakis, M. C. Asensio, A. Resta, B. Ealet, and G. Le Lay, Phys. Rev. Lett. **108**, 155501 (2012).

[11] R. Arafune, C.-L. Lin, K. Kawahara, N. Tsukahara, E. Minamitani, Y. Kim, N. Takagi, and M. Kawai, Surf. Sci. **608**, 297 (2013).

[12] E. Cinquanta, E. Scalise, D. Chiappe, C. Grazianetti, B. van den Broek, M. Houssa, M. Fanciulli, and A. Molle, J. Phys. Chem. C **117**, 16719 (2013).

[13] Z. Majzik, M. Rachid Tchalala, M. Švec, P. Hapala, H. Enriquez, A. Kara, A. J. Mayne, G. Dujardin, P. Jelínek, and H. Oughaddou, J. Phys.: Condens. Matter **25**, 225301 (2013).

[14] A. Resta, T. Leoni, C. Barth, A. Ranguis, C. Becker, T. Bruhn, P. Vogt, and G. Le Lay, Sci. Rep. **3**, 2399 (2013).

[15] C. Grazianetti, D. Chiappe, E. Cinquanta, G. Tallarida, M. Fanciulli, and A. Molle, Appl. Surf. Sci. **291**, 109 (2014).

[16] K. Kawahara, T. Shirasawa, R. Arafune, C.-L. Lin, T. Takahashi, M. Kawai, and N. Takagi, Surf. Sci. **623**, 25 (2014).

[17] P. Moras, T. O. Mentes, P. M. Sheverdyaeva, A. Locatelli, and C. Carbone, J. Phys.: Condens. Matter **26**, 185001 (2014).

[18] M. R. Tchalala, H. Enriquez, H. Yildirim, A. Kara, A. J. Mayne, G. Dujardin, M. A. Ali, and H. Oughaddou, Appl. Surf. Sci. **303**, 61 (2014).

[19] C. Léandri, H. Oughaddou, B. Aufray, J. M. Gay, G. Le Lay, A. Ranguis, and Y. Garreau, Surf. Sci. **601**, 262 (2007).

[20] M. S. Rahman, T. Nakagawa, and S. Mizuno, Jpn. J. Appl. Phys. **54**, 015502 (2015).

[21] T. Shirai, T. Shirasawa, T. Hirahara, N. Fukui, T. Takahashi, and S. Hasegawa, Phys. Rev. B **89**, 241403 (2014).

[22] A. J. Mannix, B. Kiraly, B. L. Fisher, M. C. Hersam, and N. P. Guisinger, ACS Nano **8**, 7538 (2014).

[23] R. Bernard, T. Leoni, A. Wilson, T. Lelaidier, H. Sahaf, E. Moyen, L. Assaud, L. Santinacci, F. Leroy, F. Cheynis, A. Ranguis, H. Jamgotchian, C. Becker, Y. Borensztein, M. Hanbücken, G. Prévot, and L. Masson, Phys. Rev. B **88**, 121411(R) (2013).

[24] F. Ronci, G. Serrano, P. Gori, A. Cricenti, and S. Colonna, Phys. Rev. B **89**, 115437 (2014).

[25] S. Olivier, A. Saúl, and G. Tréglia, Appl. Surf. Sci. **212-213**, 866 (2003).

[26] S. Cahangirov, M. Audiffred, P. Tang, A. Iacomino, W. Duan, G. Merino, and A. Rubio, Phys. Rev. B **88**, 035432 (2013).

[27] G. Prévot, R. Bernard, H. Cruguel, and Y. Borensztein, Appl. Phys. Lett. **105**, 213106 (2014).

[28] J. Sone, T. Yamagami, Y. Aoki, K. Nakatsuji, and H. Hirayama, New J. Phys. **16**, 095004 (2014).

[29] A. Wilson, R. Bernard, A. Vlad, Y. Borensztein, A. Coati, B. Croset, Y. Garreau, and G. Prévot, Phys. Rev. B **90**, 075416 (2014).

[30] J. P. Perdew and A. Zunger, Phys. Rev. B **23**, 5048 (1981).

[31] J. P. Perdew, K. Burke, and M. Ernzerhof, Phys. Rev. Lett. **77**, 3865 (1996).

[32] QUANTUM ESPRESSO is an open source distribution available at http://www.quantum-espresso.org; P. Giannozzi, S. Baroni, N. Bonini, M. Calandra, R. Car, C. Cavazzoni, D. Ceresoli, G. L. Chiarotti, M. Cococcioni, I. Dabo, A. Dal Corso, S. de Gironcoli, S. Fabris, G. Fratesi, R. Gebauer, U. Gerstmann, C. Gougoussis, A. Kokalj, M. Lazzeri, L. Martin-Samos, N. Marzari, F. Mauri, R. Mazzarello, S. Paolini, A. Pasquarello, L. Paulatto, C. Sbraccia, S. Scandolo, G. Sclauzero, A. P. Seitsonen, A. Smogunov, P. Umari, and R. M. Wentzcovitch, J. Phys.: Condens. Matter **21**, 395502 (2009).

[33] G. Kresse and D. Joubert, Phys. Rev. B **59**, 1758 (1999).

[34] N. Marzari, D. Vanderbilt, A. De Vita, and M. C. Payne, Phys. Rev. Lett. **82**, 3296 (1999).

[35] G. Prévot, C. Cohen, D. Schmaus, and V. Pontikis, Surf. Sci. **459**, 57 (2000).

[36] G. Boisvert and L. J. Lewis, Phys. Rev. B **54**, 2880 (1996).

[37] Z.-L. Liu, M.-X. Wang, J.-P. Xu, J.-F. Ge, G. Le Lay, P. Vogt, D. Qian, C.-L. Gao, C. Liu, and J.-F. Jia, New J. Phys. **16**, 075006 (2014).

[38] J. A. Martín-Gago, R. Fasel, J. Hayoz, R. G. Agostino, D. Naumović, P. Aebi, and L. Schlapbach, Phys. Rev. B **55**, 12896 (1997).

[39] M. Švec, P. Hapala, M. Ondráček, P. Merino, M. Blanco-Rey, P. Mutombo, M. Vondráček, Y. Polyak, V. Cháb, J. A. Martín Gago, and P. Jelínek, Phys. Rev. B **89**, 201412(R) (2014).

[40] H. Enriquez, A. Mayne, A. Kara, S. Vizzini, S. Roth, B. Lalmi, A. P. Seitsonen, B. Aufray, T. Greber, R. Belkhou, G. Dujardin, and H. Oughaddou, Appl. Phys. Lett. **101**, 021605 (2012).

[41] H. Oughaddou, S. Sawaya, J. Goniakowski, B. Aufray, G. Le Lay, J. M. Gay, G. Tréglia, J. P. Bibérian, N. Barrett, C. Guillot *et al.*, Phys. Rev. B **62**, 16653 (2000).

[42] Y. Fukaya, I. Mochizuki, M. Maekawa, K. Wada, T. Hyodo, I. Matsuda, and A. Kawasuso, Phys. Rev. B **88**, 205413 (2013).

[43] J. Venables, G. Spiller, and M. Hanbücken, Rep. Prog. Phys. **47**, 399 (1984).

[44] D. D. Chambliss and K. E. Johnson, Phys. Rev. B **50**, 5012 (1994).

[45] T. Kawagoe, T. Kotaki, T. Shibasaki, Y. Ohmori, and A. Itoh, Surf. Sci. **468**, 1 (2000).

[46] J. A. Meyer and R. J. Behm, Surf. Sci. **322**, L275 (1995).

[47] R. Pentcheva, K. A. Fichthorn, M. Scheffler, T. Bernhard, R. Pfandzelter, and H. Winter, Phys. Rev. Lett. **90**, 076101 (2003).

[48] G. Antczak and G. Ehrlich, Surf. Sci. Rep. **62**, 39 (2007).

[49] G. Prévot, C. Cohen, J. Moulin, and D. Schmaus, Surf. Sci. **421**, 364 (1999).